International Journal of Medical Imaging
2016; 4(6): 57-69
http://www.sciencepublishinggroup.com/j/ijmi
doi: 10.11648/j.ijmi.20160406.13
ISSN: 2330-8303 (Print); ISSN: 2330-832X (Online)

A BP Neural Networks Algorithm for High Resolution of Biomedical Modeling and Image Segmentation

Zheng Xiang[1], Hui Xie[2], Junhao Li[1], Zhengying Cai[1, *]

[1]College of Computer and Information Technology, China Three Gorges University, Yichang, China

[2]School of Law and Public Administration, China Three Gorges University, Yichang, China

Email address:

1137953238@qq.com (Zheng Xiang), 1446228804@qq.com (Hui Xie), 1115749422@qq.com (Junhao Li), master_cai@163.com (Zhengying Cai)

[*]Corresponding author

To cite this article:

Zheng Xiang, Hui Xie, Junhao Li, Zhengying Cai. A BP Neural Networks Algorithm for High Resolution of Biomedical Modeling and Image Segmentation. *International Journal of Medical Imaging.* Vol. 4, No. 6, 2016, pp. 57-69. doi: 10.11648/j.ijmi.20160406.13

Received: October 23, 2016; **Accepted**: November 7, 2016; **Published**: December 29, 2016

Abstract: High resolution of image segment algorithm plays a very important role in biomedical modeling and diagnosis, which is difficult to be easily solved by traditional algorithms. This article presents a biomedical image segment algorithm based on computational intelligence. First, an assessment method for image resolution is proposed here, and some related models are also compared. In addition, the assessment method aims at high resolution, rather than defining a comprehensive model of the human visual system. Second, a high resolution algorithm is illustrated where the BP neural network is trained from numerical features. The proposed approach permits person to get biomedical model with a high resolution. Third, some experimental results are presented for illustration, and the numerical analysis verifies the resolution measurement and the effectiveness of the BP neural method. Last, some interesting conclusions and future work are indicated at the end of the paper.

Keywords: High Resolution, Bio Modeling, Image Segment, Neural Networks

1. Introduction

Generally, high resolution of image segment algorithm plays a very important role in biomedical modeling and diagnosis. Therefore, many researchers devoted their energy into this area. Edison (2016) published a microwave assisted green synthesis of fluorescent N-doped carbon dots with cytotoxicity and bio-imaging applications [1]. Ni Yong (2014) gave their ideas in Far-red and near infrared BODIPY dyes with synthesis and applications for fluorescent pH probes and bio-imaging [2]. Huang (2014) conveyed their concepts in their work coumarin dye-embedded semiconducting polymer dots for ratiometric sensing of fluoride ions in aqueous solution and bio-imaging in cells [3]. Zhu (2015) introduced a twisted intramolecular charge transfer probe for rapid and specific detection of trace biological SO_2 derivatives and bio-imaging applications [4]. Goswami (2016) described a visual and near IR (NIR) fluorescence detection of Cr3+ in aqueous media via spirobenzopyran ring opening with application in logic gate and bio-imaging [5]. Chuang (2014) expressed their opinions in their work photo stimulable near-infrared persistent luminescent nanoprobes for ultrasensitive and longitudinal deep-tissue bio-imaging [6]. Ju (2015) researched a bio-inspired development of a Dual-Mode Nanoprobe for MRI and Raman Imaging in his article [7]. Sharker (2015) published their academic paper Target delivery of beta-cyclodextrin/paclitaxel complex fluorescent carbon nanoparticles with externally NIR light and internally pH sensitive-mediated release of paclitaxel with bio-imaging in 2015, and this article was a success in some manner [8]. Fan (2014) put forward a solution based synthesis of III-V quantum dots and their applications in gas sensing and bio-imaging, which was a great progress too [9]. Zhao (2015) optically investigated Nd3+-Yb3+ cascade sensitized up conversion nanoparticles for high resolution, rapid scanning, deep and damage-free bio-imaging [10].

Many novel methods were applied in biomedical image, such as nano composites. Cheng (2015) studied gold nanoparticle-enhanced near infrared fluorescent nano composites for targeted bio-imaging [11]. Yang (2015) researched one-pot one-cluster synthesis of fluorescent and

bio-compatible Ag-14 nano clusters for cancer cell imaging [12]. Zhao (2015) came up with bio-imaging and photodynamic therapy with tetra sulphonatophenyl porphyrin (TSPP)-TiO2 nano whiskers, which was a new approach einrheumatoid arthritis the ranostics [13]. Fletcher (2015) offered the latest applications of 3D ToF-SIMS bio-imaging [14]. Ghormade Vandana (2015) expressed their view that human can embed fluorescent cadmium telluride quantum dots into chitosan nanoparticles, which will be a stable, biocompatible preparation for bio-imaging [15]. Jurowski (2015) conveyed their thoughts in the thesis the analytical calibration in (bio) imaging/mapping of the metallic elements in biological samples with definitions, nomenclature and strategies with state of the art [16]. Li (2016) made a mitochondria-targeted two-photon fluorescent probe for highly selective and rapid detection of hypochlorite and its bio-imaging in living cells [17]. Mandal (2015) discovered a new pyridoxal based fluorescence chemo-sensor for detection of Zn (II) and its application in bio imaging [18]. Kono (2014) extended label free bio image sensor for real time monitoring of potassium ion released from hippocampal slices [19]. Kim (2016) immobilized rhodamine scaffold onto mesoporous silica as a fluorescent probe for the detection of Fe (III) and applications in bio-imaging and microfluidic chips [20]. Bishop (2016) introduced elemental bio-imaging using laser ablation-triple quadrupole-ICP-MS to us [21].

All these researches actually aimed at improve the image resolution, while it is very difficult to evaluate the image resolution. Hare (2016) researched high-resolution chemical imaging of bio-elements in Caenorhabditis elegans [22]. Jurowski (2015) studied bio analytics in quantitive (Bio) imaging/mapping of metallic elements in biological samples [23]. Verma (2015) put a lot of effort into researching Center symmetric local binary co-occurrence pattern for texture, face and bio-medical imageretrieva [24]. Wang (2015) published their work beta-Ga2O3, Cr3+ nanoparticle from a new platform with near infrared photoluminescence for drug targeting delivery and bio-imaging simultaneously [25]. Ganguly (2015) studied the orange-red silver emitters for sensing application and bio-imaging [26]. Hofmann (2014) presented their ideas in their work comprehensive bio-imaging using myocardial perfusion reserve index during cardiac magnetic resonance imaging and high-sensitive troponin T for the prediction of outcomes in heart transplant recipients [27]. Osminkina (2014) studied the nanoparticles prepared from porous silicon nanowires for bio-imaging and sono dynamic therapy [28]. Esposito (2014) researched the performance of a novel wafer scale CMOS active pixel sensor for bio-medical imaging [29].

This article presents a biomedical image segment algorithm coming from computational intelligence. First, an assessment method for image resolution is proposed here, and some related models are also compared. In addition, the assessment method aims at high resolution, rather than defining the human visual system's comprehensive model. Second, a high resolution algorithm is illustrated where the BP neural network is trained from numerical features. The proposed approach permits person to make biomedical model with a high resolution. Third, some experimental results are presented for illustration, and numerical analysis verifies the resolution measurement and the effectiveness of the BP neural method. Last, some interesting conclusions and future work are indicated at the end of the paper.

2. Resolution Evaluation of Bio Imaging

2.1. Block-Based Imaging Resolution

Image resolution is generally reliable and objective, but it lacks incentive to find new method for automatically measuring enhanced picture resolution. To get a high resolution of imaging scheme, it is very important to provide a template database for reference, then the selector can make resolution evaluation. The proposed high resolution imaging scheme based on BP neural networks is shown in figure 1.

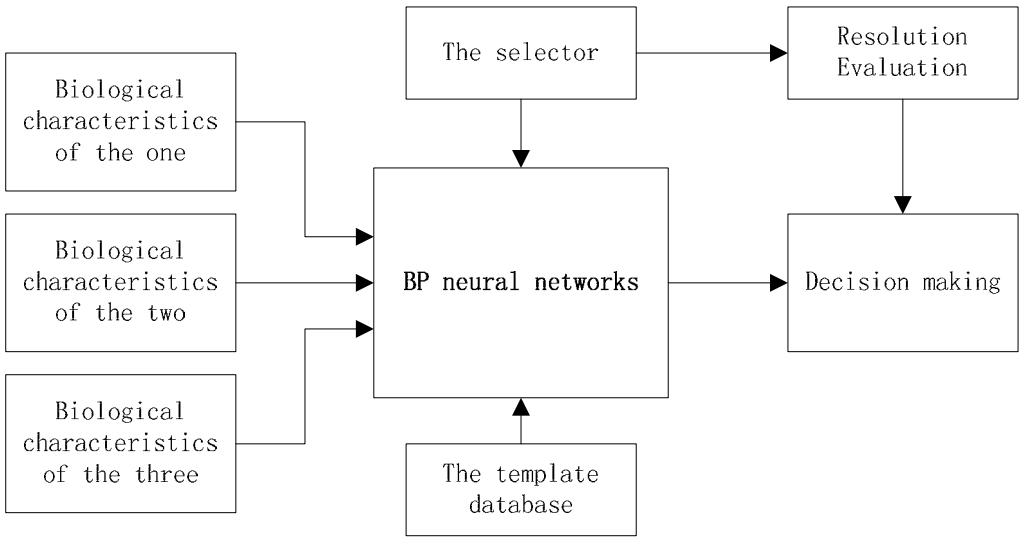

Figure 1. *High resolution scheme based on BP neural networks.*

Denoted by the space of all possible images: a filter, $\alpha()$, with the associate enhanced image: α : $(U \to U)$ and the perceptual function, $J(U, \alpha(U))$.

$$J : U \times U \to [-1, +1]. \tag{1}$$

Here the resolution score is normalized to [-1, + 1] range without loss of generality. Single model assumes that a subset of the filter (process) image *j* is actually available to the end user.

$$\text{J}: U' \to \text{ [-1,+1]}. \tag{2}$$

Problem set (2) one way [10, 11, 18-21] gives a scientific basis. Performance requirement means that any approach (2) must be carried consistently propagation of human perception, which in any case must be measured. It creates a big problem that for statistical inference, almost unlimited input space and the size of the U', but it is not feasible to make an exhaustive search method. The only way to make statistical problems of the complexity of (2) reasonable seems to reduce the data dimension space. In the field of image processing, the characteristics of the image can be used. If *j* (U) feature extraction operator mapping image space to a low dimensional feature space, H, the original problem (2) is transformed into low dimensional formula:

$$J = J_H \circ \phi, \tag{3}$$

The phenomenon of resolution assessment is mapped by an operator (1 + 1).

This study is based on the problems of target imaging resolution settings (3), as shown in figure 1. Formula (3) emphasizes the divide-and-conquer strategy implementation of the advantages of the proposed. It allows a separation complexity reduce image resolution prediction of the function of the two tasks: (1) selection, if properly selected to describe the image, the basis of the result in (2) and the mapping function of design, which is likely to be highly nonlinear unknown, even imitate the perception mechanism.

Symbols and conventions

$\zeta = \{\text{U}^{(\text{S})}; \text{s} = 1, \ldots, \text{n}_\text{p}\}$ is the collection of the original image.

$\alpha_l(\bullet)$, (l = 1;...; ne) is the n_e patient raise filter, necessary to assess the effect of its resolution.

$Y^{(U)} = \{y_q^{(U)}; q = 1, \ldots, n_y\}$ is a collection of image segmentation to get U to the n_y square.

$\varphi = \{f_m; m = 1, \ldots, n_y\}$ is to describe the image collection of target n_f characteristics.

$f_{mq}^{(s)}$ is the value of the feature $f_m \in \varphi$ for the *q*th, *s*th image block $U^{(S)} \in \zeta$.

$\overset{\cap(s,l)}{U} = \partial_l(U^{(s)})$ is the enhanced image obtained by processing $U^{(s)} \in \zeta$ from the filter.

$\overset{\cap(s,l)}{f}_{mq}$ is the feature value $f_m \in \varphi$ for the *q*th, *s*th image block $\overset{\cap(s,l)}{U}$.

The whole thesis, general practice, rounded hat symbol to measure will strengthen such filter after application.

To evaluate the image resolution in global level f_m, a statistical descriptor vector is needed.

The structure of the neural network input algorithm is as follow.

Give an image $\overset{\cap(s,l)}{U}$ which is enhanced by the *l*th filter, and then calculate the following quantities:

$$\begin{aligned} f_m^M &= median(\overset{\cap(s,l)}{f}_{m1}, \ldots, \overset{\cap(s,l)}{f}_{mn_y}), \\ f_m^S &= stdev(\overset{\cap(s,l)}{f}_{m1}, \ldots, \overset{\cap(s,l)}{f}_{mn_y}), m = 1, \ldots, n_{b,} \end{aligned} \tag{4}$$

n_y is the active features number that have been chosen for the set of B.

The vector $\vec{a}^{s,f}$ for the image $\overset{\cap(s,l)}{U}$ is

$$\vec{a}^{(s,l)} = \{f_m^M, f_m^S; m = 1, \ldots, n_b\}. \tag{5}$$

For the reason of its inherent action of robust statistics, median operator is used. In neuronal network resolution evaluating system, every image is stood by a unique input mode, which is applying the method of two steps: first, the $\overset{\cap(s,l)}{U}$ image makes an analysis based on the basis of block-by-block; second, the statistical descriptors of objective vector $\vec{a}^{(s,l)}$ has dimension $d = 2n_b$ included in the objective index of the final properties of two times. The description $Y^{(U)}$ of the image based on block can be planned according to the two distinct methods.

2.2. Pixel-Based Imaging Resolution

This kind of method comes from standardized column diagram which is the first-order, $G_q(p)$ of block $y_y^{(l)}$ measuring D x D pixels; $G_q(p)$ is reckoned as $G_q(g) = N_{qg} / D^2, p = 0, \ldots, n_l - 1.$ in which *p* represents a generic gray-level value of a pixel, n_l =256, and N_{qp} is the number of pixels in $y_y^{(l)}$ with gray level *p*.

$$\text{Mean} = \mu_p = \sum_p p G_q(p)$$

$$\text{stdev} = \sigma_p = [\sum_p (p - \mu_p)^2 G_q(p)]^{1/2}$$

$$\text{entrogy} = - \sum_p G_q(p) \log_2 G_q(p),$$

These features are come from the co-occurrence matrix ($0 \le \text{p}_\text{i}$, $p_j < n_l - 1$);

$$\text{co\_autoc} = \sum_{p_i,p_j} p_i p_j c_q(p_i,p_j,\alpha,\beta),$$

$$\text{co\_invd} = \sum_{p_i,p_j} \frac{c_q(p_i,p_j,\alpha,\beta)}{1+(p_i-p_j)^2},$$

$$\text{co\_entropy=-} \sum_{p_i,p_j} c_q(p_i,p_j,\alpha,\beta)\log_2 c_q(p_i,p_j,\alpha,\beta)$$

$$\text{co\_cow} = \sum_{p_i,p_j} (p_i-\mu_i)(p_j-\mu_j)c_q(p_i,p_j,\alpha,\beta)$$

$$(\mu_i = \sum_{p_i,p_j} p_i c_q(p_i,p_j,\alpha,\beta),\mu_j) = \sum_{p_i,p_j} p_j c_q(p_i,p_j,\alpha,\beta))$$

The following quantities are needed by the remaining features,

$$\text{P: } (\alpha,\beta) = \sum_{\substack{p_i,p_j \\ |p_i-p_j|=c}} c_q(p_i,p_j,\alpha,\beta); (0 \le c < n_l - 1).$$

Based on $P_c(\alpha,\beta)$, there are four features:

$$\text{co\_absv} = \sum_c cP_c(\alpha,\beta),$$

$$\text{co\_diffVar} = [\sum_c (c-co\_absv)^2 P_c(\alpha,\beta)^{1/2}],$$

$$\text{co\_cont} = \sum_c cP_c(\alpha,\beta).$$

$$\text{co\_diffEnt} = \text{-} \sum_c P_c(\alpha,\beta)\log_2 P_c(\alpha,\beta).$$

Other features include ($0 \le m, n < D$):

$$\text{f\_dcEn=} Y_q[0,0] / \sum_{m,n} Y_q[m,n],$$

$$\text{f\_horEn=} \sum_n Y_q[0,n] / \sum_{m,n} Y_q[m,n],$$

$$\text{f\_diagEn=} \sum_{\substack{m,n \\ m=n}} Y_q[m,n] / \sum_{m,n} Y_q[m,n],$$

where block $B_q(U)$, $B_q[m, n]$ is the constituent at the angular frequencies from m to n.

3. High Resolution Algorithm Based on BP Neural Networks

3.1. The Imaging Modelling in Biological Samples

In imaging modeling, feed forward neural network plays the role of image description based on feature mapping to a scalar value, so it should represent the image resolution. Each unit includes a simple weighted input nonlinear transformation, and theory proves that the feed forward network embedded can support arbitrary nonlinear mapping.

Circular back propagation network extends the traditional network model, by adding the square of an input value which is the sum of all the input of the network. The second increase will not affect the long-term effective attribute structure. In addition, the model of choice is completely data-driven, from the experience of training process. The connection between a hidden layer includes neurons with an s-shaped nonlinear:

$$x_v(\vec{a}) = sigm(L_{v,o} + \sum_{m=1}^{d} a_m^2).$$

$$u = 1,\ldots,n_y, \tag{6}$$

where sign ( ) = (U +),{ } is a set of coefficients or weight, often a deviation. Finally, the symbols represent the truth neuron stimulation and activation, respectively. Output layer provides *b*, that is, the final response.

$$b(\vec{a}) = sigm(L_0 + \sum_{v=1}^{n_h} L_v x_v(\vec{a})), \tag{7}$$

where { } is on behalf of the output coefficient and output deviation, respectively.

Neural network can be seen as the weight of nonlinear computing devices to set their own freedom, and the training process can adjust the coefficient of such networks for input/output mapping. For this purpose, in addition to the simplest case, a formula of input/output behavior can be used to describe the input mode of training set and they expect response.

For a given set of weights, *L* describes a neural network, the performance cost measures on the training set mapping accuracy. Therefore, the network training process can be expressed as

$$\min_L E_L = \min_L \frac{1}{n_r} \sum_{s=1}^{n_r} [t^{(s)} - b(\vec{a}^{(s)})]^2, \tag{8}$$

where $t(s)$ and $y(\vec{a}^{(s)})$ denote the base of training set, and network outputs, respectively.

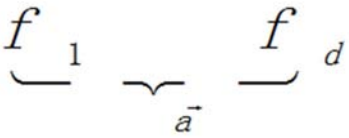

Figure 2. *The additional input augments the feed forward architecture.*

An estimator of prediction is always with some mistakes, because the sample is attracted to form a training set of statistical fluctuations. A typical method to increase reliability is to replace single neural stage. The estimate can be described as a bias decomposition.

$$\varepsilon^2 = \delta^2 + \theta^2. \tag{9}$$

Deviations decomposition may not be appropriate estimation model, in that, results in a fixed offset can be measured. Variance (θ^2) is as a result of the training data statistical noise, and it can be minimized by simple average.

As a result, the parallel use of several network (figure 2) can help minimize the overall variance of the imaging resolution. These descriptors of a set of $\overline{\theta}^2 = \theta^2 / N$ statistical independence elements can be ideally reduced in estimation variance. Such a simple method has been successful.

However, the key problem is to obtain such the estimate of imaging modelling. The easiest way is to oppose such that in the training the data can be randomly divided into *a* set of disjoint subsets element as much as possible, to make sure there is no correlation. This requires a lot of sample, the more frequently the solution is to be trained in different net, the better such work in the same data set can get. But from the planning, the design optimization process is different in initial parameter types. The disadvantages of this method, is the estimation can often prove to be highly correlated. Don't usually subspace intersection, the local average results of the estimation provides an overall estimate. These subvectors form training set are for each of the network as a whole. Cognitive theory is the data space partition causing global estimation such tasks in a coordinate, and imaging modelling.

Design problem of an estimator, is to prove its effective at run time eventually include training model complexity, the minimum to be maintained. In fact, considering the generalization problem, it is very difficult to design such a system. In addition, some experience proved it to be successful in the standard [24], especially in a real application. To set up the literature does not provide theory instruction, but also shows the practicality.

3.2. The BP Neural Networks for Imaging Segment

In imaging segment, it is important to measure the brightness of the image content distribution, spatial orientation, frequency energy distribution, and so on. They can be divided into different families: characteristics of first-order to be extracted from the histogram of the image block, description of the level of grey probability distribution in a picture. C(g_i, g_j, α, β) said the co-occurrence matrix represents the probability distribution of pixels and gray levels and, respectively, by the radial unit in the horizontal axis. So, features from C(g_i, g_j, α, β) is an effective structure characterization properties [24, 25].

To extract the feature subset may be trivial or superfluous to describe main parts of the image, which will determine the perception of the resolution. This study USES statistical methods to choose only those features, carries most of the information of image enhancement filter effects on perceived resolution.

Analysis from the complete set of features H selects the statistics only a subset of the active characteristics. Function is active statistical properties which vary significantly from the original value after the application of an enhanced filter. H is for each target characteristics analysis and comparison, therefore, the statistical features of two samples: one contains the value of a set of original parameters from unfiltered images, the other has the values of a set of enhanced image. To ensure the two samples are statistical independent, two groups of images are not intersected.

The two data sets come from the same population. Feature selection algorithm can be summarized as follows.

For each objective characteristic $f_m \in \varphi, m = 1, \ldots, n_j$, each picture $U^{(s)} \in \zeta, S = 1, \ldots, n_r$,

- Use the n_e filters, to divide each resulting image, including the initial ones, into n_b blocks, and to calculate the complete set of feature values, Ω_m :

$$\Omega_m = \bigcup_{s=1}^{n_r} \{\{f_{mq}^{(s)}; q = 1, \ldots, n_y\} \cup \{\overset{\cap(s,l)}{f}_{mq}; l = 1, \ldots, n_e; q = 1, \ldots, n_y\}\}, \quad \in m = 1, \ldots, n_j. \tag{10}$$

Then it is to count the .05 and the .95 percent, namely $a_{.05}^{(m)}$ and $a_{.95}^{(m)}$, severally, for the numeral values in Ω_m.

For the construction of data set, each enhanced filter ($l = 1, \ldots, n_e$).

- To create two sets not joint, $\zeta_1^{(l)} \cap \zeta_2^{(l)} = \varnothing$

Each resulting is generated from randomly extracting $n_d \le n_p / 2$ from images ζ.

- To use the filter α_l for each element of $\zeta_2^{(l)}$

to gain $\overset{\cap(l)}{\zeta}_2 = \{\overset{\cap(e,l)}{U}; \forall U^{(e)} \in \zeta_2^{(l)}\}$.

Then it is to calculate each feature $f_m \in \varphi$ ($m = 1, \ldots, n_f$) for each image, and produce the sets $\Lambda_{1m}^{(l)}$ and $\Lambda_{2m}^{(l)}$

$$\begin{aligned} \Lambda_{lm}^{(l)} &= \{f_{mq}^{(e)}; \forall U^{(e)} \in \zeta_1^{(l)}; q \in B^{(U^{(e)})}\}, \\ \overset{\cap(e,l)}{\Lambda}_{2m} &= \{\overset{\cap(e,l)}{f}_{mq}; \forall \overset{\cap(e,l)}{U} \in \overset{\cap(l)}{\zeta}_2; q \in B^{(U^{(e,l)})}\}. \end{aligned} \tag{11}$$

Assuming $B^{(a)}$ is the set of n_y, which is a non-overlapping block to be obtained from the Image *a*.

- To standardize each $\Lambda_{lm}^{(l)}$ and $\overset{\cap(l)}{\Lambda}_{2m}$ into the scope [-1,1]

$$\begin{aligned} f_{-mq}^{(e)} &\overset{def}{=\!=} 2\frac{(f_{mq}^{(e)} - a_{.05}^{(m)})}{(a_{.95}^{(m)} - a_{.05}^{(m)})} - 1, \\ \overset{\cap(e,l)}{f}_{-mq} &\overset{def}{=\!=} 2\frac{(\overset{\cap(e,l)}{f}_{mq} - a_{.05}^{(e)})}{(a_{.95}^{(e)} - a_{.05}^{(e)})} - 1. \end{aligned} \tag{12}$$

Make $\Lambda_{lm}^{(l)}$ and $\overset{\cap(l)}{\Lambda}_{2m}$ become the orthonormal sets of (7), singly,including the values counted in (8).

As Kolmogorov- Smirnov test, it is to gather a probability vector, $\vec{r}$, described as

$$r[m,l] = p_{ms}(\Lambda_{lm}^{(l)}, \overset{\cap(l)}{\Lambda}_{2m}); \quad m = 1, \ldots, n_f; l = 1, \ldots, n_e \tag{13}$$

In which $r_{ms}(\bullet, \bullet)$ is the important consequence of the

image test beneath the invalid theory where the data sets $\Lambda_{lm}^{(l)}$ and $\overset{\cap(l)}{\Lambda}_{2m}$ have been gained from the same distribution.

As ranking of feature,

- To set the reference confident threshold, for example

$$r^{*}=0.1$$

- To count the pointer vector, $\vec{t}$, as

$$f[m,l]=\begin{cases}1 & r[m,l]\le r^{*}\\ 0 & r[m,l]>r^{*}\end{cases}\quad m=1,\ldots,n_f;\qquad (14)$$

$$l=1,\ldots,n_e,$$

- To converge the occurrence vector $\vec{o}$, whose *element numbers M*, through all likely filters, from the event where the databases $\Lambda_{1m}^{(l)}$ and $\overset{\cap(l)}{\Lambda}_{2m}$ are not gotten from the same distribution. Therefore, $0\le o[e]\le n_e$, and

$$o[e]=\sum_{l=1}^{n_e}t[e,l],e=1,\ldots,n_{f.}\qquad (15)$$

To gather the last feature set by all these features f_m for which $o[m]$ it up to a threshold, $o^{*}\le n_e$:

$$f_m\in Y\Leftrightarrow o[m]\ge o^{*}.\qquad (16)$$

A group of characteristics are gathered in the statistical features of *Y*, so the algorithms significantly changed the characteristics of enhanced filter. Filter threshold value can determine the number of events according to the statistical properties of properties change may enhance filter to allow a choice. Its value experience, because of its shape depends on $o[m]$, and the results expected the support on the dimensions of the final validation group *B* from the objective image resolution evaluation and the performance of the whole system.

Feature selection algorithm uses the information of the original image, but overall still can be seen as a single objective method. In fact, the image segment only helps choose a set of important function of filter, and such a choice should be done only at startup. At runtime, these features are to be assessed from the enhanced image, continuously training neural network to estimate related resolution score.

4. Application and Instruction

In practical application, neural imaging resolution and this model test are through the use of a patient of contrast enhancement filter. Filter is used to adjust the brightness of the image.

Enhance pixel belongs to a region containing significant details. This algorithm can modify a pixel brightness value using the following procedure.

From the area, around 5x5 considering pixels are employed to decide the local contrast DL estimated around the pixel brightness changes, and the brightness of the local variance of S which is an indication of the amount of high spatial frequency. Here M pixel brightness and contrast level are the average brightness in the surrounding area.

Set the brightness of the pixel value as

$$M^{new}=M_e+(M^{old}-M_e)G,G=f(\Delta M,S,\rho,\sigma)\qquad (17)$$

In which G is 0 or 1. G value depends upon two parameters: *t*, local contrast threshold.

It prevents the humble number in detail, and further enhances the high contrast image area, where the main is very detailed, and low contrast areas need to be enhanced. In a word, the filter depends upon three parameters: two thresholds of ρ and σ , and a gain value of α . In the current study, ρ spanned over three values, { ρ_n ; n = 1,...,3}, σ varied over two values (σ_e ; e =1,2}, and α changed from five values { ϕ_m ; m= 1,...,5}. As a consequence, the patient $\alpha_l(l=1,\ldots,n_e)$ on enhancement filters is to be assessed in the experiments of resolution evaluation comprised with n_e=30 members.

In practice, enhanced filters may have more complex image, such as a process of a library of n_i =16 (252 x 189 pixels in size) gray-scale images, whose contents changed from natural images to patterns which are texture-like. Using the set of n_e= 30 contrast enhance filters, as being defined in (17), to the patient of n_i =16 the initial image to produce samples of 480 enhanced image. Enhancement could produce a perceived resolution, which was higher and lower about the enhanced image. When it is compared with the initial one, scoring scale is double-ended applied, where the bad side shows enhanced images becoming worse than the initial image, while the good side shows enhanced images becoming better than the initial one.

In order to provide the subjects, a lot of granularity at both ends of the disjoined scale is applied, such as an 11-point numeric scale changing from -5 to +5. Then the regularization is scaled into the scope [-1;1] making those scores consistent with the output representation of the neural-network. Full set of 480 enhanced image evaluation is based on a study by more patients participate in subgroup where most patients need high resolution of bio images.

Analysis of bio images needs more participants in each group provided by 10 or more enhanced image resolution score. Because this analysis requires a lot of subjects, the experiment can be run on the Internet. To adjust the spatial resolution of the display, the user requirement, the number of color standard setting and judge the image viewing distance, are usually on the computer monitor application.

5. Experimental Results

5.1. Experiment Background

For illustration, several imaging experiments were made to

verify the proposed BP neural algorithm. To compare the statistical methods before, the behavior of the target features $f_m \in \varphi$ over a set of images, $\overset{\cap(s,l)}{U}$ are observed. For each image, the analysis of the statistical features of comparing two samples: the sample characteristic value of the first overlaps block, while the second sample contains the value of the same function overlap block. For each feature $f_m \in \varphi$ of subset of each image, overlapping value calculation block has a pair of image tests. This experiment provides a fragment, and the result of the image test importance level is given as a subset of the four images. The filter settings are different in a patient table.

The empirical results provide strong evidence that in addition to small exceptions, the null hypothesis cannot be rejected. Therefore, they can be reasonably asserted that in most cases, two samples and overlap ping are involved, respectively, appearing to come from the same population. Resolution, therefore, to assess the feature extraction process, system, overlapping strategy, selecting this option will need a smaller computational overhead.

5.2. Experimental Results

The feature selection process described in the third quarter defines the input vector of the neural network system. Figure 3 lists the result set (4) of descriptive function. These descriptors depend on two parameters, namely *J* and *o*. Experiment with fixed value $j = 2$, which means that the co-occurrence matrix is always calculated in two pixels neighborhood radius. This setting is measured by using large radius values to evaluate the relative advantage. Experiments showed that the settings did not offer significant advantages, but only implied the calculation burden. Angular orientation parameters, *o* was across eight main directions. This led to a number $n_b = 8$ of selection functions. As a result, the final input space dimension for neural network was amounted to d =2^ n_b = 256.

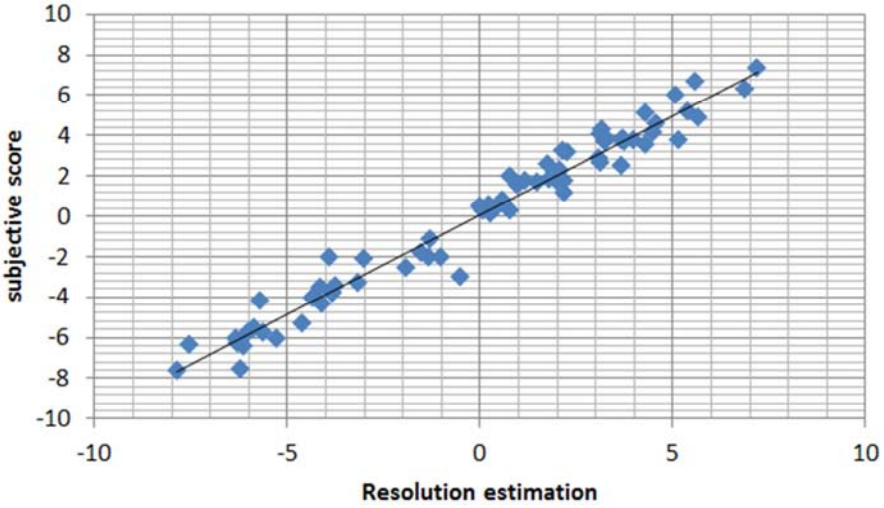

Figure 3. *Resolution estimation of proposed model.*

Cross validation method measured the performance of the resolution evaluation system. Sample available was randomly divided into training set and test set, including enhanced image in illness diagnosis. In the system setup and training process, only the training set was used, and the test set was specially used to measure the generalization ability of bio image system.

As the input space was a pretty big dimensionality, compared with the sample size of enhanced image training set, a whole strategy is needed to use an input space division and professional network. In evaluation system design, there is N = 8 in different neural networks, so each set elements are entrusted with specific Angle positioning of co-occurrence matrix. As the input space partition, it shows that the input vector of the elements of each set includes four characteristics parameterized by $\beta = \beta_i$. This reduces the neural network input space to $d_i = 4$. For each collection element, the number of hidden layer neurons was empirically set to N_h = 4. Increasing the number of neurons takes not obvious advantage.

Diagram in figure 4 shows the error distribution of mass fraction of ensemble estimator of the validation set according to reference [10], [22]. From the scatter diagram in figure 4, an objective resolution estimate is given as concentration data points around the diagonal of the plot to confirm good searching performance of the neural network assessment system for random validation group of images.

The correlation coefficient is equal to the whole system 0.91, but the error of average prediction was 0.13% and the average absolute prediction error was 0.75%. Drawn in figure 4, the (*j, j*) experimental error distribution axis is compared with an ideal corresponding of Gaussian distribution, $N(\overset{\cap(Ens)}{\mu_{err}}, s_{err}^{(Ens)})$ on the axis.

Two axes express that their respective data sets, each point (*j, j*), horizontal distribution are the same. Chart shows that the estimate of the error distribution in mass fraction can be a normal distribution model, pointing about distribution along the dotted line.

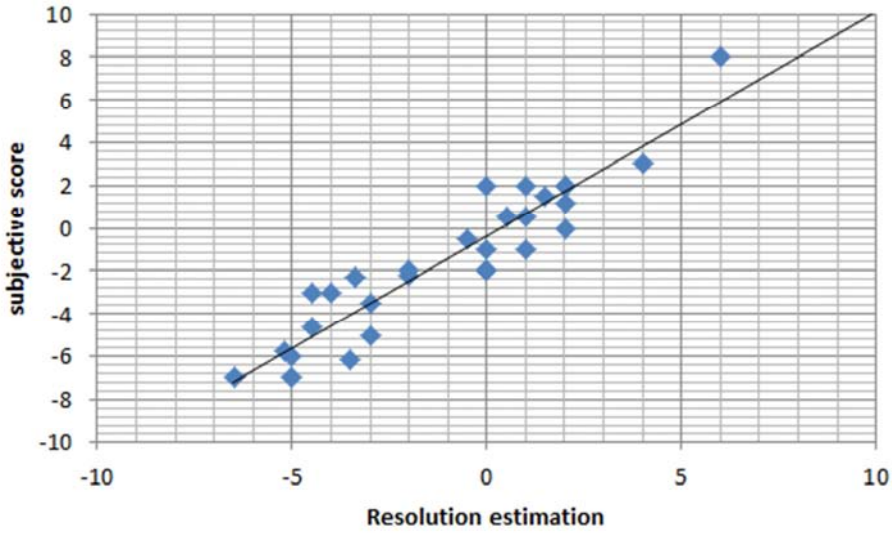

Figure 4. *Resolution estimation of reference.*

As shown in figure 5, integration of the neural network searching performance estimates a new set of original image including scatterplot estimation resolution value, subjective scores, (*j, j*) plot comparison error estimates of score distribution ($\overset{\cap}{\mu}_{err}^{(Ens)}, s_{err}^{(Ens)}$).

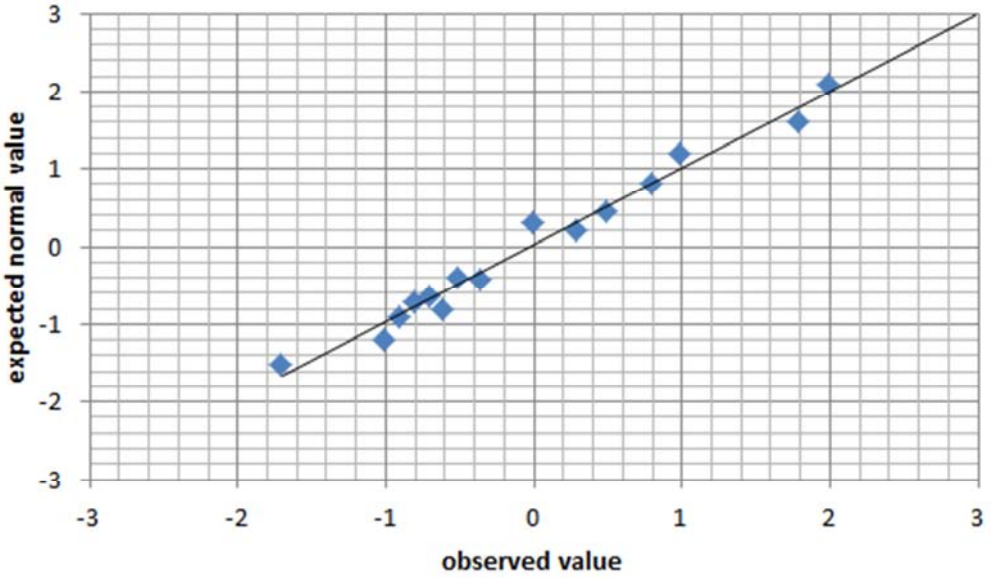

Figure 5. *Observed resolution of proposed model.*

Description above and figure 5 show that the evaluation method can achieve satisfactory searching performance of a set of the original image and it is not used in neural network settings. Also, it seems to be interesting to check the searching performance of neural based evaluation system in the use of different sets of enhanced filters. These tests are designed to verify whether training network measures the contrast enhancement image of the resolution, or, estimate whether the system is suitable to diagnose the nature of his illness, as enhanced filter (17) described in the section 3.1.

This next experiment result using a gray-scale images from reference [10], [22] is presented in figure 6, but now deals with a different bio image, *p*, of the filter.

Compared with the original filter y/patient, patient g different set parameters is obtained, which is across a new scope $\{ \bar{\delta}_m; m = 1,\ldots,4 \}$. Less key parameters, *t* and *l* respectively presented three values $\{ \rho_n; n = 1,\ldots,3 \}$ and two values $\{ \alpha_e; e = 1,2 \}$. As a consequence, $\bar{\alpha}_i(\mathrm{i},\ldots, n_e)$ patient comprised a set of characteristics to diagnose the nature of his illness.

This set of filter was applied to the diagnosis of the original image, and produced a new sample = 8 x 4 = 32 of enhanced image as an extra panel testing. Nervous resolution assessment system did not change with the change of the section 5.3 in resolution score.

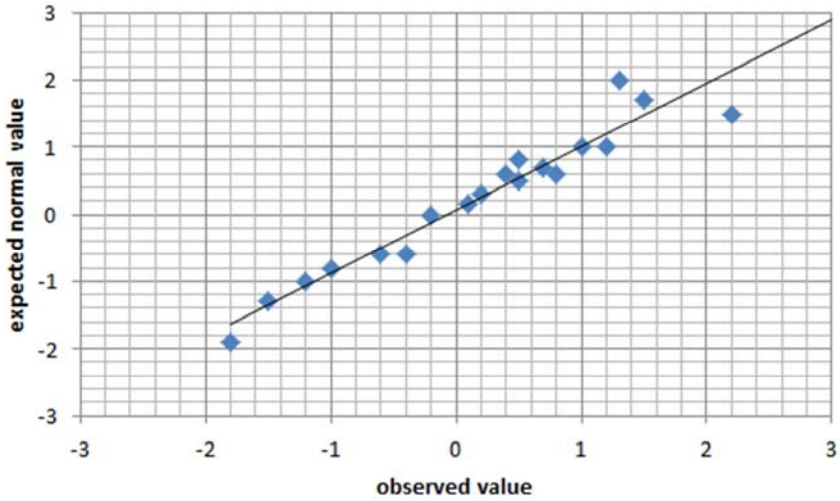

Figure 6. *Observed resolution of reference.*

5.3. Further Analysis

For further discussion, the stimulation of the training set and testing set were enhanced by applying for the same filter α_l of the same sample set of the original images. Therefore, there is correlation between two data sets, the corresponding relationship between training set and test set may affect the reliability of the results. The resolution changes of proposed model and reference models are compared in figure 7 and 8.

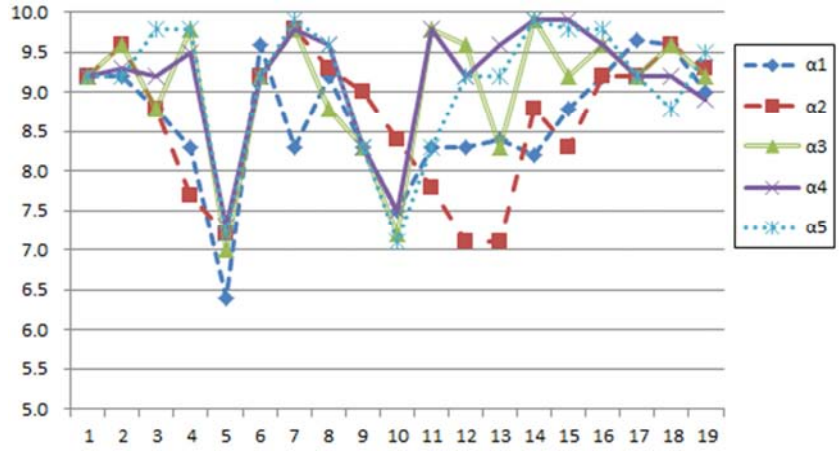

Figure 7. *The resolution change of proposed model.*

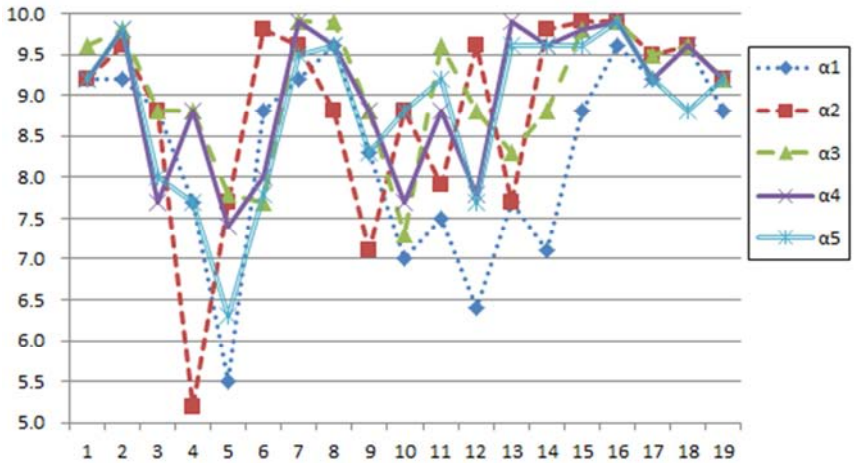

Figure 8. *The resolution change of reference.*

As above, Figure 7 and Figure 8 showed the resolution changes of proposed model and reference model for enhanced images. In figure 7 higher resolution over figure 8 displays image resolution scores of the overall estimate of error distribution. Scatter diagram in figure 7 is given to estimate the objective resolution of bio image. Around diagonal plot, the concentration of the surrounding data points confirmed the satisfaction of neural network searching performance by applying the new enhancement of image filters $\bar{\alpha}_i$. The whole system has reached the Pearson correlation coefficient equal to 0.91, but the error of average prediction was 0.15% and the error of mean absolute prediction was 7.2%.

As the parameter β, the comparison of proposed model and reference model in bio image are shown in figure 9, and 10 respectively.

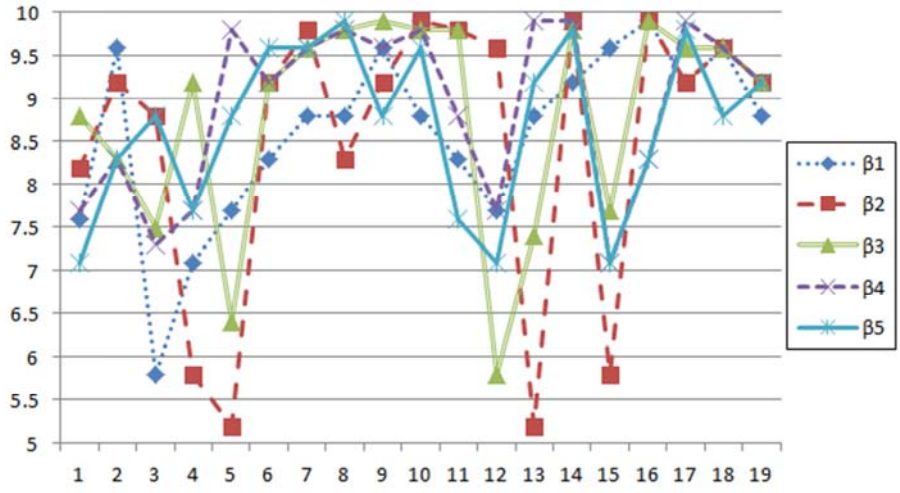

Figure 9. *The resolution change of proposed model.*

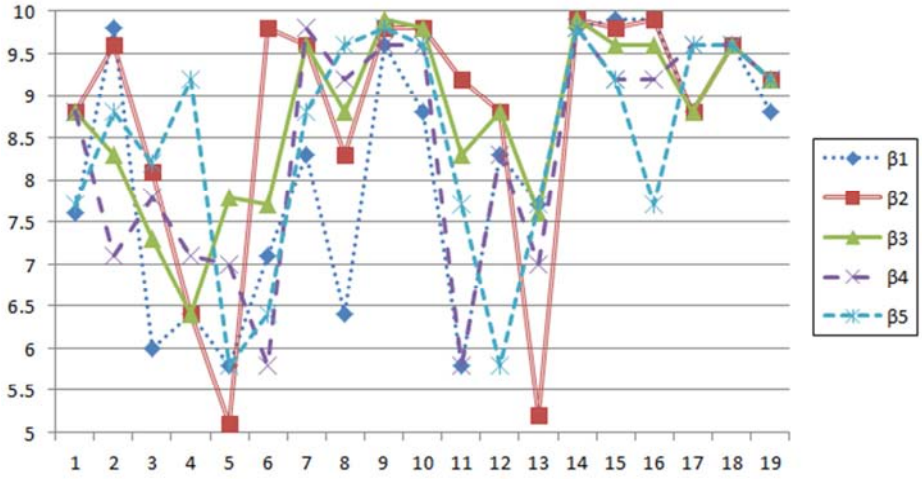

Figure 10. *The resolution change of reference.*

As can be seen from figure 9 and figure 10, the resolution changes with β are more stable than α in figure 7 and 8. The setting of the searching performance of integrated neural estimator image is processed by a image filter of the contrast enhancement scatterplot, to estimate the resolution value and subjective scores. (*j, j*) plot compared error estimates of score distribution ($\hat{\mu}_{err}^{(Ens)}$, $s_{err}^{(Ens)}$.) axis and the corresponding results of an ideal Gaussian distribution. N ($\hat{\mu}_{err}^{(Ens)}$, $s_{err}^{(Ens)}$) in experience, $n(y)$, is the Gaussian parameters measurement of the mean and variance values. Two axes expressed in plot units of each point (*j, j*) plot, and the horizontal distribution is the same. Chart shows the estimate of the error distribution of mass fraction can be in normal distribution model, because the point distribution is along the dotted line.

This intellectual property with enhanced redistribution, allows many application and collaborations for illness diagnosis activities for hospital and biopharmaceutical companies. It can help bio image specialization in developing bioassays and selling proprietary to hospital or clinic, biopharmaceutical companies and medical research institutions. Bioassays can also developed by neural networks on a contract service basis.

As the parameter δ, the comparison of proposed model and reference model are shown in figure 11, and 12 respectively. The effectiveness of the method is based on the performance of each ensemble estimates, $\{c_i, i = 1,\ldots,4\}$.

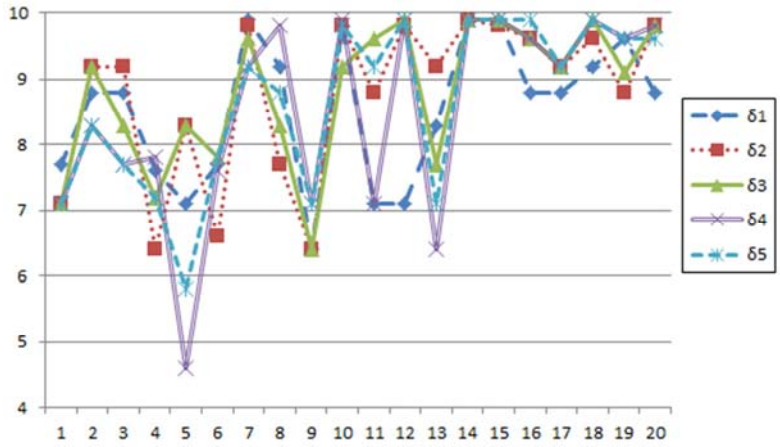

Figure 11. *The resolution change of proposed model.*

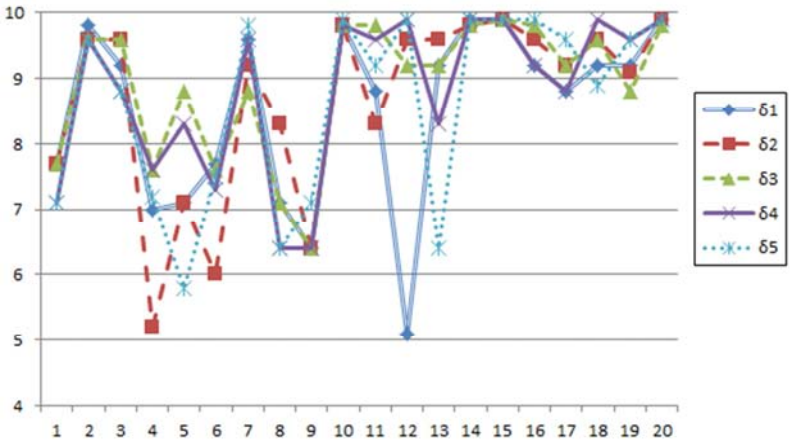

Figure 12. *The resolution change of reference.*

As shown in figure 11 and figure 12, the δ value returned as mass fraction by neural network, δ was compared with the actual mass fraction, and t, was collected by the human evaluation. As expected, the comparison of all cross validation on test set was performed. Shown in figure 12, image filter for this experiment consisted of $n_e = 4$ members, after filtration, it can enhance the image collection to $n_r = n_i \times n_e = 16$ images. Enhanced image is used to perform a subjective test, as described in section 5.1, and the objective assessment of neural network perception of image resolution evaluation and image segment system.

This section summarizes the performance results of each image segment with same main neural parameters to estimate the whole ensemble ($c_1 - c_4$) and the validation set. This confirms that ensemble estimator improves the performance of the bio image segment, because there are fewer errors than individual estimates. In addition, a user support is available for providing basic diagnosis support. The archives of the neural network resolution can still be helpful at the old data mining and diagnosis of stubborn disease.

6. Conclusions

The resolution evaluation of the bio image segment and image modeling is traditionally difficult which can not be solved by traditional methods. In this article, a high resolution system has been put forward, which is based on a neural network and it is taken as a kind of enhancement filter to estimate the resolution of image of single variable method. The proposed method includes two aspects, to look for features to describe enhanced images, and to define a neural network for image resolution evaluation. In principle, the proposed model can extract the characteristics of different types of bio image corresponding to the nature of the image content. Additionally it is in accord with human perceive images way also, and the adaptive strategy based on feature extraction diminishes the risk of overall research.

For future research, the neural network architecture in neural network should be extended to provide us more flexible tool to simulate more complex revolution process of bio characteristics. Additionally, it is more helpful for us to prove a whole diagnosis scheme and treating strategy with improved neural network. For a large number of bio images, it is important to build an intelligent image modeling system with neural network evaluation and provide enough high resolution for color image, and to produce statistical report according to patient requirements.

Acknowledgements

This research was supported by the National Natural Science Foundation of China (No. 71471102), and Science and Technology Research Program, Hubei Provincial Department of Education in China (Grant No. D20101203).

References

[1] Edison, Thomas Nesakumar Jebakumar Immanuel; Atchudan, Raji; Sethuraman, Mathur Gopalakrishnan; Microwave assisted green synthesis of fluorescent N-doped carbon dots: Cytotoxicity and bio-imaging applications; Journal Of Photochemistry And Photobiology B-Biology, 161, (2016), 154-161.

[2] Ni, Yong; Wu, Jishan; Far-red and near infrared BODIPY dyes: synthesis and applications for fluorescent pH probes and bio-imaging; Organic & Biomolecular Chemistry; 12, (2014), 3774-3791.

[3] Huang, Ya-Chi; Chen, Chuan-Pin; Wu, Pei-Jing; Coumarin dye-embedded semiconducting polymer dots for ratiometric sensing of fluoride ions in aqueous solution and bio-imagijng in cells; JOURNAL OF MATERIALS CHEMISTRY B; 2, (2014), 6188-6191.

[4] Zhu, Leiming; Xu, Junchao; Sun, Zhe; A twisted intramolecular charge transfer probe for rapid and specific detection of trace biological SO2 derivatives and bio-imaging applications; Chemical Communications;51, (2015), 1154-1156.

[5] Goswami, Shyamaprosad; Das, Avijit Kumar; Maity, Anup Kumar; Visual and near IR (NIR) fluorescence detection of Cr3+ in aqueous media via spirobenzopyran ring opening with application in logic gate and bio-imaging; Dalton Transactions; 43, (2014), 231-239.

[6] Chuang, Yen-Jun; Zhen, Zipeng; Zhang, Fan; Photostimulable Near-Infrared Persistent Luminescent Nanoprobes for Ultrasensitive and Longitudinal Deep-Tissue Bio-Imaging; Theranostics; 4, (2014); 1112-1122.

[7] Ju, Kuk-Youn; Lee, Sangyeop; Pyo, Jung; Bio-inspired Development of a Dual-Mode Nanoprobe for MRI and Raman Imaging; SMALL; 11, (2015), 84-89.

[8] Sharker, Shazid Md.; Kim, Sung Min; Kim, Sung Han; Target delivery of beta-cyclodextrin/paclitaxel complexed fluorescent carbon nanoparticles: externally NIR light and internally pH sensitive-mediated release of paclitaxel with bio-imaging; Journal Of Materials Chemistry B; 3, (2015), 5833-5841.

[9] Fan, Guangyin; Wang, Chenyu; Fang, Jiye; Solution-based synthesis of III-V quantum dots and their applications in gas sensing and bio-imaging; NANO TODAY; 9, (2014), 69-84.

[10] Zhao, Yuxiang; Zhan, Qiuqiang; Liu, Jing; Optically investigating Nd3+-Yb3+ cascade sensitized upconversion nanoparticles for high resolution, rapid scanning, deep and damage-free bio-imaging; Biomedical Optics Express; 6, (2015), 838-848.

[11] Cheng, Hao; Wang, Chuanxi; Xu, Zhenzhu; Gold nanoparticle-enhanced near infrared fluorescent nanocomposites for targeted bio-imaging; RSC Advances; 5, (2015), 20-26.

[12] Yang, Jie; Xia, Nan; Wang, Xinan; One-pot one-cluster synthesis of fluorescent and bio-compatible Ag-14 nanoclusters for cancer cell imaging; Nanoscale; 7, (2015), 18464-18470.

[13] Zhao, Chunqiu; Rehman, Fawad Ur; Yang, Yanlong; Bio-imaging and Photodynamic Therapy with Tetra Sulphonatophenyl Porphyrin (TSPP)-TiO2 Nanowhiskers: New Approaches in Rheumatoid Arthritis Theranostics; Scientific Reports; 5, (2015).

[14] Fletcher, John S; Latest applications of 3D ToF-SIMS bio-imaging; BIOINTERPHASES; 10, (2015).

[15] Ghormade, Vandana; Gholap, Haribhau; Kale, Sonia; Fluorescent cadmium telluride quantum dots embedded chitosan nanoparticles: a stable, biocompatible preparation for bio-imaging; JOURNAL OF Biomaterials Science-Polymer Edition; 26, (2015), 42-56.

[16] Jurowski, Kamil; Buszewski, Boguslaw; Piekoszewski, Wojciech; The analytical calibration in (bio) imaging/mapping of the metallic elements in biological samples - Definitions, nomenclature and strategies: State of the art; TALANTA; 131, (2015), 273-285.

[17] Li, Daoxue; Feng, Yan; Lin, Jizhi; A mitochondria-targeted two-photon fluorescent probe for highly selective and rapid detection of hypochlorite and its bio-imaging in living cells; Sensors And Actuators B-Chemical; 222, (2016), 483-491.

[18] Mandal, Senjuti; Sikdar, Yeasin; Maiti, Dilip K; A new pyridoxal based fluorescence chemo-sensor for detection of Zn (II) and its application inbio imaging. RSC Advances; 5, (2015), 72659-72669.

[19] Kono, Akiteru; Sakurai, Takashi; Hattori, Toshiaki; Label free bio image sensor for real time monitoring of potassium ion released from hippocampal slices; Sensors And Actuators B-Chemical; 201, (2014), 439-443.

[20] Kim, Hyungjoo; Rao, Boddu Ananda; Jeong, Jaemyeng; A rhodamine scaffold immobilized onto mesoporous silica as a fluorescent probe for the detection of Fe (III) and applications in bio-imaging and microfluidic chips; Sensors And Actuators B-Chemical; 224, (2016), 404-412.

[21] Bishop, David P.; Clases, David; Fryer, Fred; Elemental bio-imaging using laser ablation-triple quadrupole-ICP-MS; Journal Of Analytical Atomic Spectrometry; 31, (2016), 197-202.

[22] Hare, Dominic J.; Jones, Michael W. M.; Wimmer, Verena C.; High-resolution complementary chemical imaging of bio-elements in Caenorhabditis elegans; Metallomics; 8, (2016), 156-160.

[23] Jurowski, Kamil; Buszewski, Boguslaw; Piekoszewski, Wojciech; Bioanalytics in Quantitive (Bio)imaging/Mapping of Metallic Elements in Biological Samples; Critical Reviews In Analytical Chemistry; 45, (2015), 334-347.

[24] Verma, Manisha; Raman, Balasubramanian; Center symmetric local binary co-occurrence pattern for texture, face and bio-medical imageretrieval; Journal Of Visual Communication And Image Representation; 32, (2015), 224-236.

[25] Wang, Xin-Shi; Situ, Jun-Qing; Ying, Xiao-Ying; beta-Ga2O3: Cr3+ nanoparticle: A new platform with near infrared photoluminescence for drug targeting delivery and bio-imaging simultaneously; ACTA Biomaterialia; 22, (2015), 164-172.

[26] Ganguly, Mainak; Jana, Jayasmita; Das, Bodhisatwa; Orange-red silver emitters for sensing application and bio-imaging; Dalton Transactions; 44, (2015), 11457-11469.

[27] Hofmann, N. P.; Steuer, C.; Voss, A; Comprehensive Bio-Imaging Using Myocardial Perfusion Reserve Index During Cardiac Magnetic Resonance Imaging and High-Sensitive Troponin T for the Prediction of Outcomes in Heart Transplant Recipients; American Journal Of Transplantation; 14, (2014), 2607-2616.

[28] Osminkina, Liubov A.; Sivakov, Vladimir A.; Mysov, Grigory A.; Nanoparticles prepared from porous silicon nanowires for bio-imaging and sonodynamic therapy; Nanoscale Research Letters; 9, (2014).

[29] Esposito, M.; Anaxagoras, T.; Konstantinidis, A. C.; Performance of a novel wafer scale CMOS active pixel sensor for bio-medical imaging; Physics In Medicine And Biology; 59, (2014), 3533-3554.